# DESIGN OF LOW COST, HIGHLY ADSORBENT ACTIVATED CARBON FIBERS

**18 March 2003**

**Sponsored by**

**Defense Advanced Research Projects Agency**
**(Defense Sciences Office)**

**ARPA Order Nr. D611, Amdt 47**

**Issued by U.S. Army Aviation and Missile Command Under**
**Contract No. DAAH01-99-C-R175**

**Effective Date of Contract: 08 June 1999**
**Contract Expiration Date: 31 July 2002**



DISCLAIMER

"The views and conclusions contained in this document are those of the authors and should not be interpreted as representing the official policies, either express or implied, of the Defense Advanced Research Projects Agency or the U.S. Government."

# REPORT DOCUMENTATION PAGE

*Form Approved*
*OMB No. 0704-0188*



| 1. REPORT DATE *(DD-MM-YYYY)* | 2. REPORT TYPE | 3. DATES COVERED *(From - To)* |
|---|---|---|
| 17-03-2003 | FINAL | Jun 1999 - Jul 2002 |

**4. TITLE AND SUBTITLE**
Design of Low Cost, Highly Adsorbent Activated Carbon Fibers

**5a. CONTRACT NUMBER**
DAAH01-99-C-R175

**5b. GRANT NUMBER**

**5c. PROGRAM ELEMENT NUMBER**

**6. AUTHOR(S)**
Mangun, Christian, L

**5d. PROJECT NUMBER**

**5e. TASK NUMBER**

**5f. WORK UNIT NUMBER**

**7. PERFORMING ORGANIZATION NAME(S) AND ADDRESS(ES)**
EKOS Materials Corporation
101 Tomaras Avenue
Savoy, IL 61874

**8. PERFORMING ORGANIZATION REPORT NUMBER**

**9. SPONSORING/MONITORING AGENCY NAME(S) AND ADDRESS(ES)**
U.S. Army Aviation & Missile Command
Mr. Phillips, Tech Monitor
Bldg. 7804, Room 212
Redstone Arsenal, AL 35898-5248

**10. SPONSOR/MONITOR'S ACRONYM(S)**
AMSAM-RD-WS-DP-SB

**11. SPONSOR/MONITOR'S REPORT NUMBER(S)**
A004

**12. DISTRIBUTION/AVAILABILITY STATEMENT**
"Approved for public release; distribution unlimited."

**13. SUPPLEMENTARY NOTES**

**14. ABSTRACT**
U.S. troops and civilians face increasing risk of exposure to chemical and biological threats as developing nations and terrorist groups turn to these lower cost weapons for their arsenals. EKOS has developed a novel activated carbon fiber (ACF) that combines the low cost and durability of GAC with tailored pore size and pore surface chemistry for improved defense against chemical agents. ACF has another key advantage as it can be manufactured in a wide variety of product forms that allows for design flexibility (hoods, masks, parkas, handkerchiefs). In addition, EKOS demonstrated the potential to utilize carbon coated sub-micron glass fibers to replace both components of the current gas mask (HEPA filter and bed of GAC) to greatly reduce pressure drop and achieve filtration/adsorption in a single step. Finally, designed structures obtained through computational fluid dynamics were built through stereolithography (honeycomb and octet truss) then coated with activated carbon to examine a unique strategy for next generation gas masks.

**15. SUBJECT TERMS**
activated carbon fibers; gas masks; adsorbents; chemical warfare; collective protection

| 16. SECURITY CLASSIFICATION OF: | | | 17. LIMITATION OF ABSTRACT | 18. NUMBER OF PAGES | 19a. NAME OF RESPONSIBLE PERSON |
|---|---|---|---|---|---|
| a. REPORT | b. ABSTRACT | c. THIS PAGE | | | Mangun, Christian, L |
| U | U | U | UU | 23 | 19b. TELEPHONE NUMBER *(Include area code)* (217) 356-7162 |

The current data obtained on adsorption of cyanogen chloride (blood agent which prevents normal utilization of oxygen by the cells) and DMMP (toxic nerve agent) indicate that modification of the micropores can be an effective method for increasing capacity. The overall objective of the Phase II SBIR effort was to develop low cost activated carbon fibers (ACF) as a more effective adsorbent for removal of chemical warfare agents. Additional design work was required to minimize airflow resistance while retaining the necessary contact efficiency for rapid adsorption. As described in the Phase II proposal, three different strategies were explored for next generation gas masks: 1) substitution of tailored ACFs for the current ASZM-TEDA carbon utilized in gas masks, 2) carbon coating of High Efficiency Particulate Arrestor (HEPA) media to combine aerosol filtration and adsorption in a single step, 3) unique designed structures obtained through computational fluid dynamics which can filter/adsorb with tailored pressure drops. These samples were tested at the U.S. Army Edgewood RD&E Center.

## Ceramic Composites Inc.

*Furnace Construction*

A split tube furnace was designed and built for EKOS to accommodate samples up to 15" wide by ~48" long rolled up to fit within the tube. The tube has a 6" ID and 36" heated length with an approximate uniform flat zone of ±3°C temperature control. The tube is made of Inconel 601 alloy and has hinged, water-cooled end caps. The end caps include o-ring seals and atmosphere couplings for gas inlet and outlet. The furnace shell consists of fibrous alumina insulation and Kanthal A-1 heating elements embedded in half round ceramic plate heaters. The maximum temperature capability of these elements is 1100°C. The furnace shell is split horizontally and hinged with counter-balancing to allow easy opening for faster cool down after the activation cycle is complete. The gas flow system features controls for up to four inert gases and is capable of flowing any combination of the four gases during the program cycle.

*Designed Filter Structures*

CCI received a CAD file from Tensegra, Inc. of a disk shaped octet truss filter structure. The disk dimensions are 1/4" thick by 1.25" diameter. The basic building block of the octet truss structure is a triangular pyramid with the struts defining the edges of the pyramid. The design sent to CCI has a 6:1 aspect ratio (length of strut:diameter of strut) with a 500 micron truss diameter and 3mm truss length.

In previous testing, Tensegra determined that a 6:1 or 7:1 aspect ratio was the most effective for filtering micron sized particles and spores in air. The struts were coated with a hydrogel to improve capture and retention of particulates. The pore size for this geometry is approximately 3 mm. A stack of 10 "cassettes" (approximately 3") were used for testing. Pressure drop through this stack was 6.25 mm water at a face velocity of 12 cm/sec. For comparison, the HE1021 HEPA filter material from Hollingsworth and Vose (relatively low pressure drop for HEPA media) with a thickness of approximately 0.016" has a pressure drop of about 10 mm water at a

face velocity of 12 cm/sec. Tensegra claimed the capture efficiency of the stack coated with hydrogel was very high, but specific numbers were not discussed.

The rationale for using a very open cell filter is to achieve high particulate capture at very low pressure drop. These filters perform better in the high face velocity regime where turbulence, and therefore, contact efficiency with hydrogel coated struts is greater. However, to achieve the high capture efficiency, a relatively thick stack must be used, thus compactness of design is sacrificed.

In addition to this structure, CCI designed a modified honeycomb filter structure, consisting of an array of honeycomb cells. The wall thickness of the honeycomb cells is ~350 microns and the diameter of the cells (approximate pore size) is 1.5 mm. To avoid having passages straight through the thickness of the disk sample, the honeycomb cells are shifted by half a cell width every 1 mm of depth. Air entering the disk will flow through the top hex-cells. The flow is then split into three cells as it enters the second 1 mm of offset hex-cells. This is meant to cause turbulence and high contact efficiency between toxic agents in the airflow and the activated carbon hex walls. Table 1 compares geometric parameters relevant to airflow resistance and contact efficiency of the Tensegra octet truss and the offset honeycomb structures.

Table 1. Physical property characteristics of two designed filter structures.

| **Design** | **Approx. Pore Size** | **Pore Vol. Fraction** | **Surface Area/Solid Vol.** | **Surface Area/Vol. Extent** |
|---|---|---|---|---|
| Tensegra Octet Truss | 3 mm | 0.785 | 80.0 $cm^2/cc$ | 17.3 $cm^2/cc$ |
| Offset Honeycomb | 1.5 mm | 0.670 | 66.2 $cm^2/cc$ | 22.1 $cm^2/cc$ |

The objective of this work was to fabricate these designed structures in a ceramic material that can withstand the activation process of the polymeric coating. As an initial step, the octet truss structure from Tensegra and the offset honeycomb structure were fabricated using the commercial epoxy-based photoresin that came with the stereolithography machine. Stereolithography fabrication was successful on the first attempt.

Fabrication using the alumina-filled photoresin took several attempts to get the build parameters correct (especially the linear shrinkage factor). Initial work on these structures produced very fragile specimens with a success rate of only about 1 out of 4. Modifications were made to the stereolithography resin formulation and resulted in improved build success, such that every synthesis resulted in a successful part. Several of each structure have been fabricated and were sintered prior to shipping to EKOS for carbon coating.

The filter samples were scaled oversize by 16.5% such that after sintering the diameter is 1.125", suitable for testing using the breakthrough apparatus at Edgewood. The figure below shows the two different structures before firing.

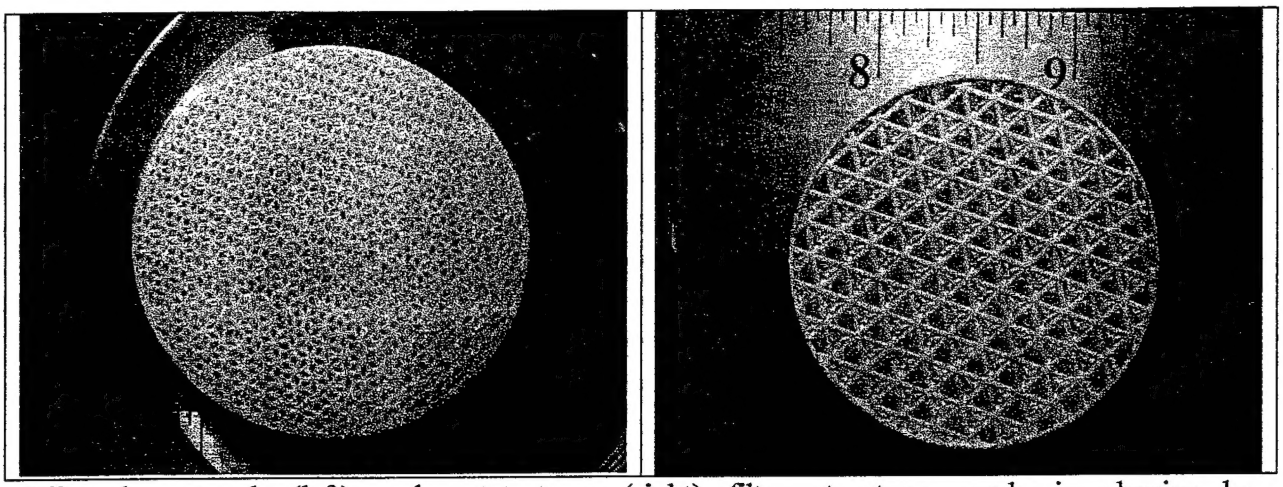


Offset honeycomb (left) and octet truss (right) filter structures made in alumina by stereolithography.

## CFD Research Corporation

*Project Scope*

Overall project activities for CFDRC were to:

- Develop and validate a 2D CFD model for fluid flow and mass transfer through gas mask filters.
- Use the model to perform a series of parametric simulations to study adsorption-pressure drop trade-offs and optimize fiber parameters.
- Use three-dimensional CFD to model flow through designed filter structures.

The project budget was expended on the first two activities. The remainder of this report describes the development of the models for adsorption and pressure drop and the application of those models to predict the performance of coated fibers.

### Model Formulation

*Governing Equations*

Flow of gas through a filter medium is governed by the equations of conservation of mass and momentum. The mass conservation equation is

$$\frac{\partial \rho}{\partial t} + \nabla \bullet (\rho u) = S_m$$

where $\rho$ is the gas density, $u$ is the velocity and $S_m$ is the adsorbate loss to the adsorbing material and is calculated by the adsorption process model discussed below. An additional equation is required for the adsorbate concentration in the gas phase

$$\frac{\partial C}{\partial t} + (u \bullet \nabla)C = \nabla \bullet D_g \nabla C - S_m$$

The momentum conservation equation is

$$\frac{\partial u}{\partial t} + (u \bullet \nabla)u = \frac{\nabla p}{\rho} + \nabla \bullet \nu \nabla u + S_u$$

$S_u$ is the source term due to momentum resistance offered by the adsorption bed. This term gives rise to the pressure drop across the bed or filter material and is calculated by the filter resistance model discussed below.

The equations above were solved using CFDRC's CFD-ACE general purpose fluid flow solver, adapted to include the adsorption model and resistance model discussed below.

*Adsorption Process*

Two different models were investigated for modeling the accumulation of adsorbent in the adsorbing medium. These were

1. Homogenous solid diffusion model (HSDM); and
2. Pore diffusion model.

Because of its relative simplicity compared to the Pore diffusion model (requiring fewer experimentally determined parameters) the HSDM was selected for implementation. In this model the adsorbate accumulates in the fibers according to a one-dimensional transient diffusion equation

$$\frac{\partial q}{\partial t} = \nabla \bullet D_s \nabla q$$

where q is the adsorbate concentration in the adsorbent and $D_s$ is an effective diffusion coefficient representing adsorbate transport within the adsorbent. This equation can be implemented for a spherical coordinate system to represent granular adsorbent or in a cylindrical coordinate system to represent fibrous adsorbing media. Both coordinate systems were implemented including a cylindrical model with a non-zero inner radius of the adsorbing material to represent the EKOS concept of an adsorbing coating on a glass fiber.

A boundary condition for the adsorbent diffusion equation in the form of a concentration at the adsorbent surface is required. This can be obtained from an equilibrium adsorption condition of the general form

$$q_s = f(C_\infty, P, T)$$

where $C_\infty$ is the bulk adsorbate concentration in the surrounding gas, $P$ is the gas pressure and $T$ is the gas temperature. Initially the Dubinin equation [1] was implemented in CFD-ACE. This equation is

$$\log_{10} q = \log_{10} q_0 - M \log_{10}^2 (P_0 / P)$$

where $q_0$ and $M$ are experimentally determined parameters. Physically, $q_0$ is indicative of the micropore volume of the adsorbent. The software was structured so that alternative equilibrium adsorption functions could also be easily implemented.

The adsorption model was tested by applying it to published results of adsorption of ammonia onto untreated activated carbon fibers [2]. Three different fiber types were modeled and the model predictions of adsorbate breakthrough are compared with the published results in Figure 1.

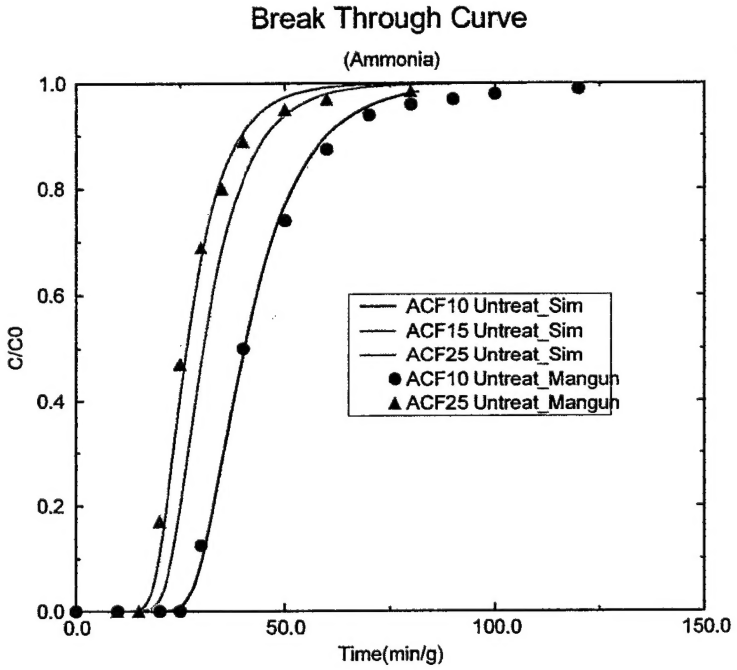


Figure 1. Prediction of ammonia adsorption on different activated carbon fibers

The model was also exercised to demonstrate its ability to respond to variation of different parameters such as gas diffusion coefficient, micropore volume and other quantities. The variation of the gas-phase concentration profile through the filter with time and with gas-phase diffusion is shown in Figure 2. The different colors represent the diffusion profile at different times and the effect of gas-phase diffusion is clearly to increase axial dispersion. Figure 3 shows the variation of bed breakthrough with variation of the parameter $q_0$, representing micropore volume. Increasing and decreasing micropore volume has nearly a linear effect on breakthrough time.

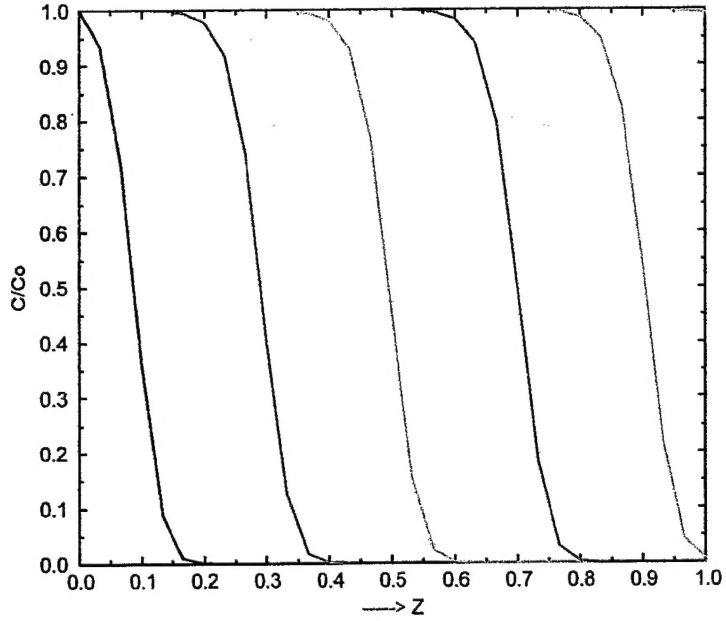


a. Without axial dispersion

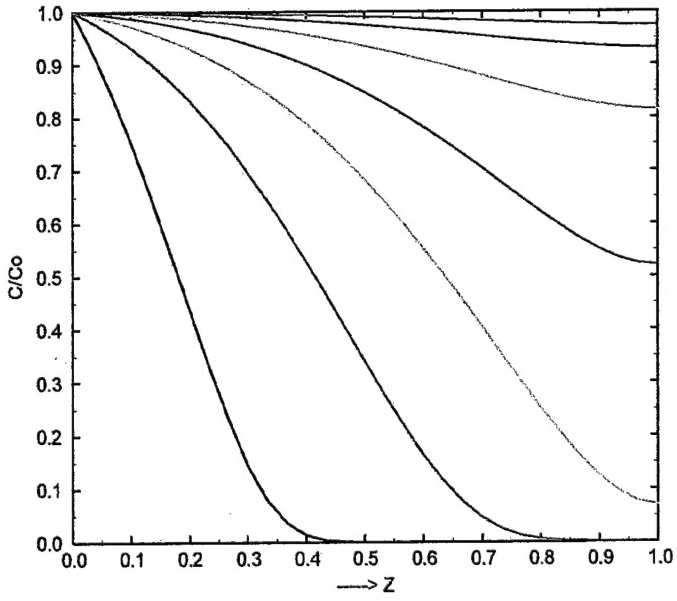


b. With axial dispersion

Figure 2. Effect of axial dispersion on time-dependent adsorption front (ammonia in ACF).

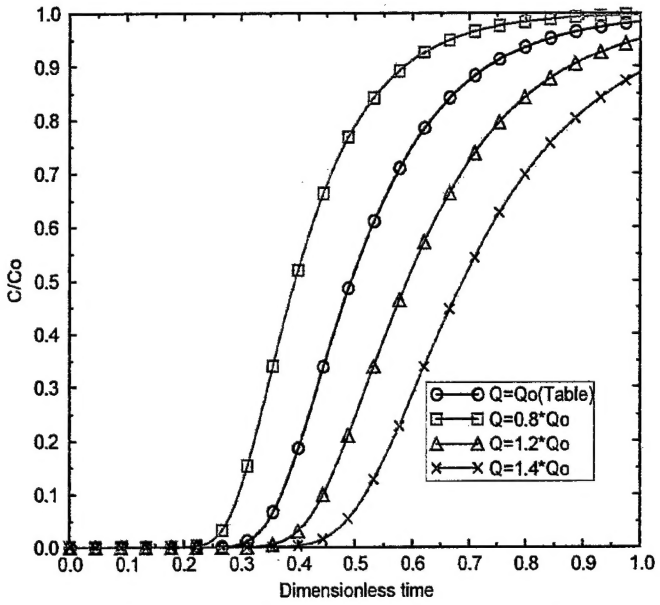


Figure 3. Effect of micropore volume (as reflected by parameter $q_0$)

*Filter Resistance Model*

Darcy's Law [3] was used to model the resistance to flow through the filter material. This is given by the equation

$$\frac{dP}{dx} = \frac{\Delta P}{L} = \frac{\mu U}{K}$$

where, $\Delta P$ = pressure drop
$L$ = bed length
$K$ = permeability
$\mu$ = viscosity
$U$ = fluid velocity

with $U$, the fluid velocity, given simply by

$$U = \frac{\dot{m}}{\rho A}$$

There are several models available for the permeability K. The first considered for this application was the Hydraulic Radius model [3,4]. The hydraulic radius, $d_h$, is defined as

$$d_h = \frac{4 * void\_vol}{surface\_area} = \frac{4\varepsilon}{A_0(1-\varepsilon)}$$

with $A_0$ being the ratio of solid surface area to solid volume and $\varepsilon$ being the external void fraction.

The permeability, $K$, is given by

$$K = \frac{\varepsilon^3 d_h^{\,2}}{16 k_k (1-\varepsilon)^2}, k_k = f(\varepsilon, \tau)$$

where $k_k$ is an empirically obtained function of void fraction, $\varepsilon$, and tortuosity, $\tau$. For the large void fractions of the filter materials anticipated for gas mask applications, the tortuosity is expected to play only a minor role. More important is the variation of surface area as fiber diameter is changed. This model is capable of responding to that change in surface area.

The qualitative effect of filter void fraction on predicted pressure drop is shown in Figure 4 where we see an exponential decrease in pressure drop as bed void fraction increases. This would, however, correspond to a decrease in adsorptive capacity due to the reduction in adsorbate mass.

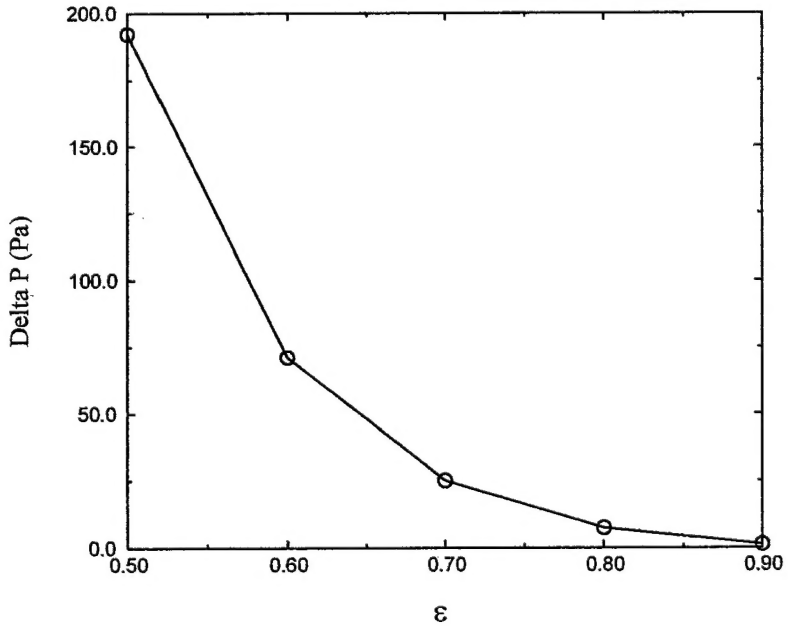


Figure 4. Effect of external void fraction on pressure drop

The previous formulation includes two empirical factors, $k_k$ and $\tau$, which we would prefer not to deal with. Therefore, an alternative formulation with less empiricism was also considered. From Darcy's law, pressure drop per bed length is

$$\frac{\Delta P}{L} = -\frac{\mu U}{K}$$

If we introduce a friction coefficient, $f$,

$$f = d\frac{\left(\frac{\Delta P}{L}\right)}{\rho U^2}$$

then the relationship between $f$ and $K$ is

$$K = \frac{1}{f}\left(\frac{d^2}{\mathrm{Re}}\right)$$

where, $d$ = fiber diameter
$\rho$ = density
Re = $\rho U d/\mu$

According to Kyan, et. al.[5], we can express the friction coefficient, $f$, as

$$f = 16k'\left[\frac{(1-\varepsilon)^2}{\mathrm{Re}\,\varepsilon^3}\right]$$

with

$$k' = \frac{(62.3Ne^2(1-\varepsilon)+107.4)\varepsilon^3}{16Ne^6(1-\varepsilon)^4}$$

and

$Ne$ = $[2\pi/(1-\varepsilon)]^{0.5}$ - 2.5
$\varepsilon$ = porosity or external void fraction

then

$$\frac{\Delta P}{L} = f\frac{\rho U^2}{d}$$

Therefore, once we fix porosity, $\varepsilon$, bed length, $L$, and fluid velocity, $U$, then we can predict $\Delta P$ as a function of fiber diameter, $d$.

Figure 5 shows a sample pressure drop prediction plot for various flow velocities assuming $\varepsilon =$ 0.95 and $L$ = 1 cm. These curves show that the variation of fiber diameter can account for a significant variation in pressure drop through a fibrous bed. Additionally, the order of magnitude was consistent with samples tested.

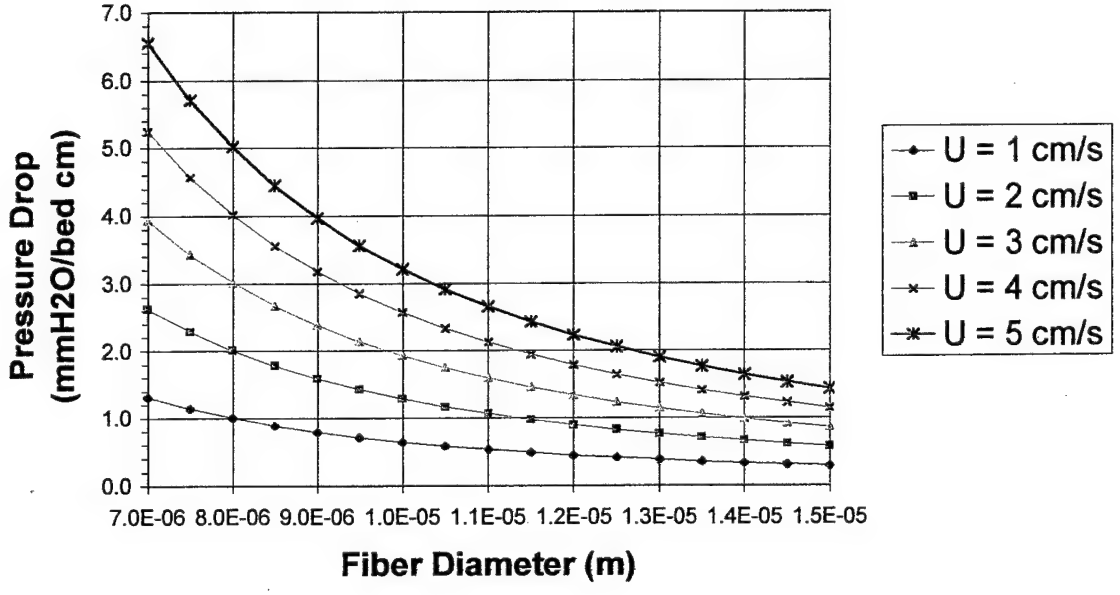


Figure 5. Variation of Pressure Drop with Fiber Diameter at Various Velocities

Finally, several additional correlations were considered. There are a multitude of correlations available for predicting pressure drop due to flow through fibrous beds [6]. All of them we mention here can be cast in the common form

$$\Delta p = \frac{2}{\pi} C_d \,\mathrm{Re} \frac{\alpha}{(1-\alpha)} \frac{\mu V L}{{d_f}^2}$$

where

| | | |
|---|---|---|
| $p$ | = | pressure |
| $C_d$ | = | drag coefficient |
| Re | = | Reynolds number |
| $\alpha$ | = | fiber volume fraction |
| $\mu$ | = | gas viscosity |
| $V$ | = | gas superficial velocity |
| $L$ | = | bed thickness |
| $d_f$ | = | fiber diameter |

The various expressions then differ only in how they express the drag coefficient $C_d$. For four expressions we wish to look at here we have

Chen:

$$\frac{C_d}{2}\mathrm{Re}=\frac{k_4}{\ln(k_5\alpha^{-0.5})}$$

Davies:

$$\frac{C_d}{2}\mathrm{Re}=16\pi(1-\alpha)\alpha^{0.5}(1+56\alpha^3)$$

Iberall:

$$\frac{C_d}{2}\mathrm{Re}=\frac{4\pi}{3}\frac{4-\ln(\mathrm{Re})}{2-\ln(\mathrm{Re})}$$

Langmuir:

$$\frac{C_d}{2}\mathrm{Re}=4\pi B(1-\alpha)\phi$$

where $k_4 = 6.1$, $k_5 = 0.64$, $B = 1$ and $\phi$ is given by

$$\frac{1}{\phi}=-\ln\alpha+2\alpha-\frac{\alpha^2}{2}-\frac{3}{2}$$

All of the relations except for Iberall's include terms that account for fiber interaction. At a porosity of 0.95 where we expect little fiber interaction, and an approach velocity of 5 cm/s they all predict similar pressure drops (agreeing to within a factor of two) as shown in Figure 6. Some test data obtained by Iberall are also shown which fall near the average of the predicted pressure drops.

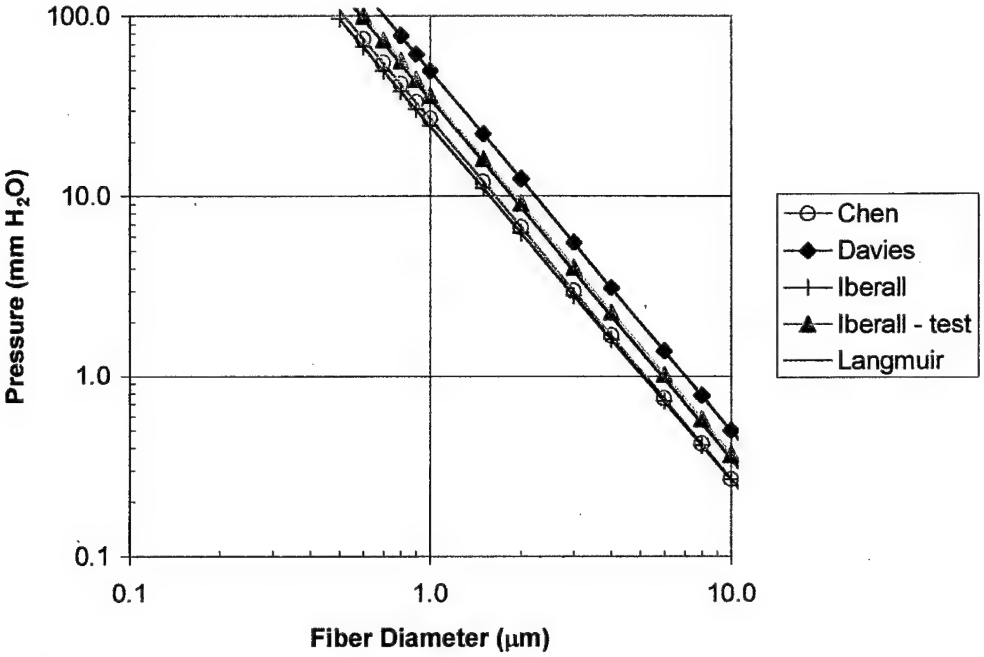


Figure 6. Pressure drop predictions at a velocity of 5 cm/s and a porosity of 0.95

At lower porosities where we expect the fiber interaction to play a more significant role the Iberall relationship starts to differ significantly from the others. In Figure 7 the Iberall relationship is compared to that of Chen for porosities ranging from 0.7 to 0.95. The lower the porosity the greater the disparity between the predictions of the two relations.

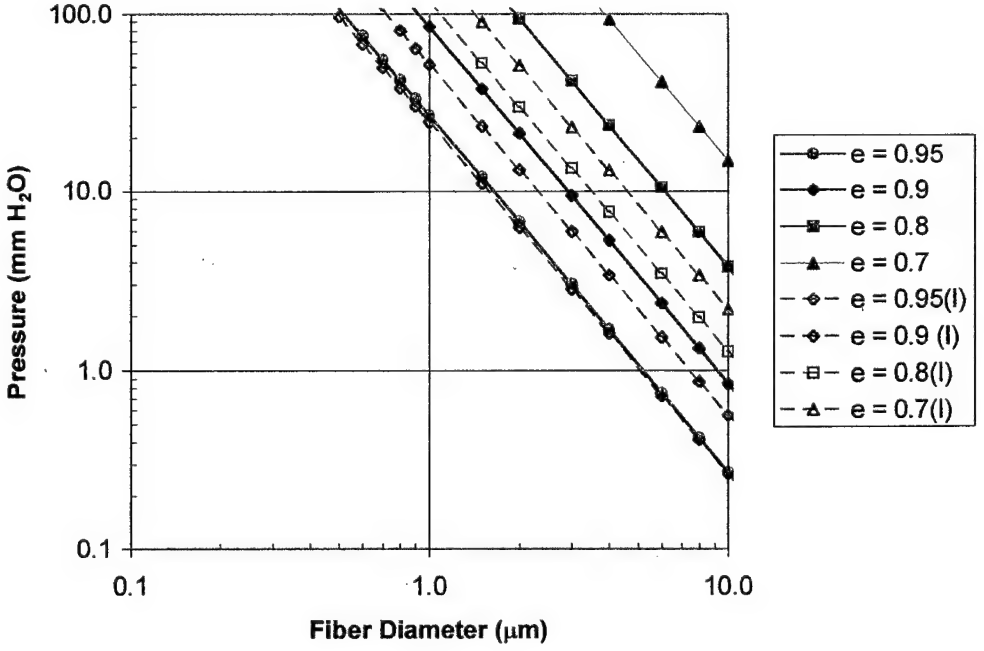


Figure 7. Comparison of Chen and Iberall (I) relations for pressure drop at a velocity of 5 cm/s and varying porosity.

However, the other relations tend to provide similar predictions as porosity changes as shown by Figure 8 where the Chen and Langmuir relations are compared over the same range of porosities as used for the Chen-Iberall comparison.

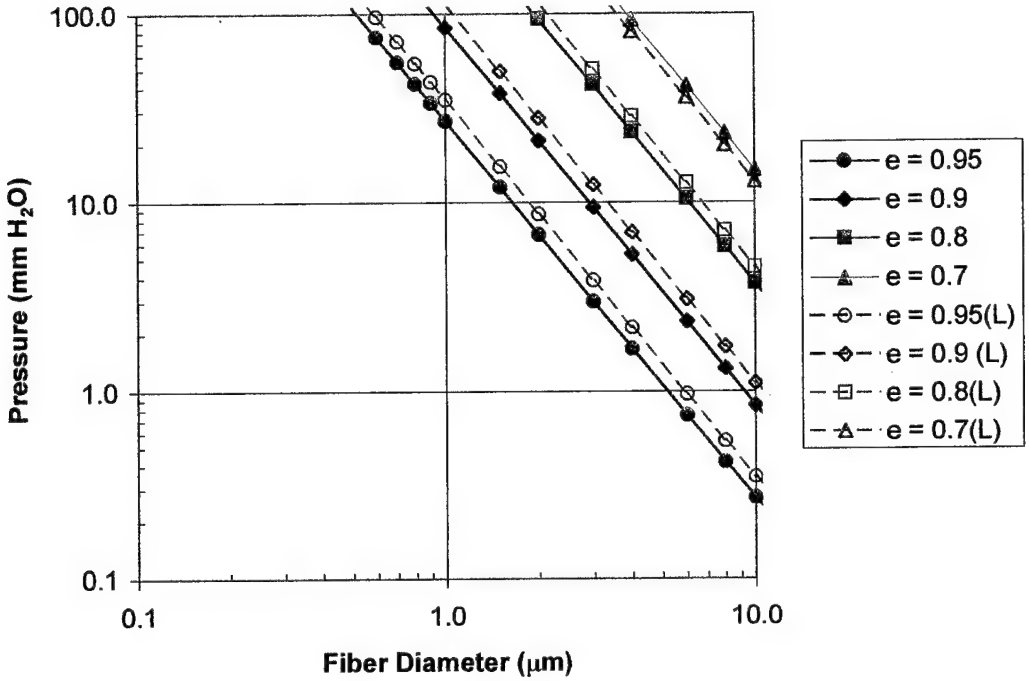


Figure 8. Comparison of Chen and Langmuir (L) relations for pressure drop at a velocity of 5 cm/s and varying porosity.

The lesson to learn here is simply that the Iberall relation, which ignores fiber interaction, should not be used. The other three relations we show here (and probably others) should be able to provide reasonable predictions.

## Results

### *Effect of Coating on Pressure Drop*

In coating glass fibers with resin we are simply moving from one porosity curve to another while changing the fiber diameter. For example, if a volume of resin equal to the glass volume is added and the starting porosity is 0.95 then the porosity of the coated web will be 0.9. Assuming homogeneous fiber diameter before and after coating, the change in fiber diameter will be $\sqrt{2}$ times the original diameter. We can then use any one of the "reasonable" pressure drop relations to calculate a pressure drop before and after coating as shown in Figure 9 (where the Langmuir relation is used). This figure gives a qualitative look at the increase in pressure drop that might be incurred by the particular circumstances described. The same procedure can easily be applied to other circumstances. The simple lesson to be learned from Figure 9 is that the higher the

pressure drop of the uncoated mat (or the smaller the original fiber diameter) the greater will be the pressure drop penalty due to coating.

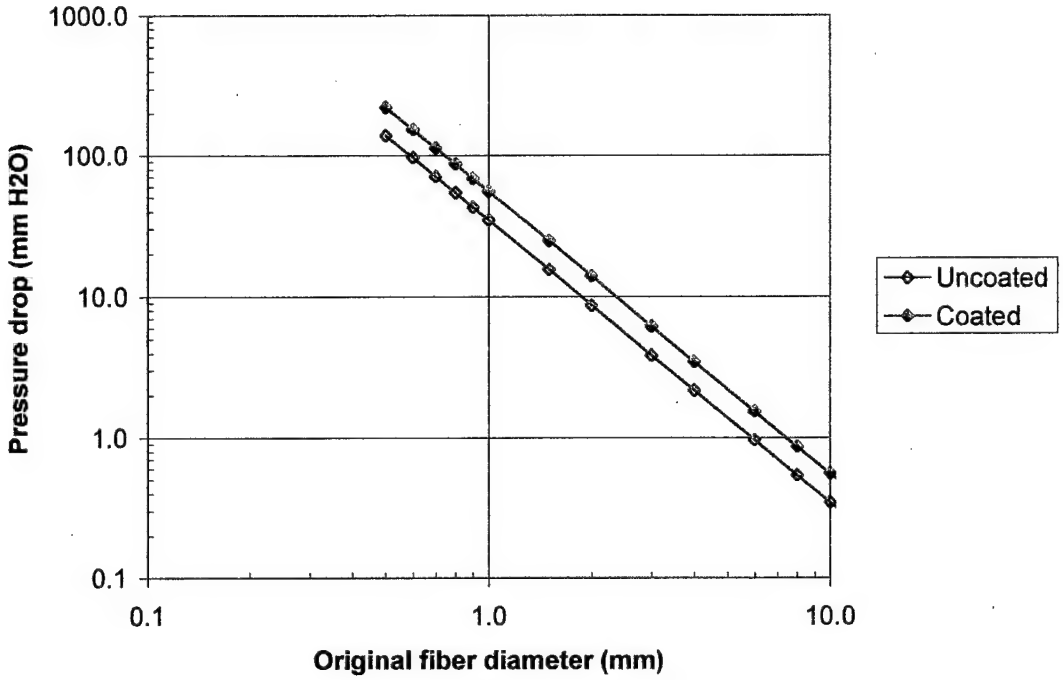


Figure 9. Pressure drop through uncoated ($\varepsilon = 0.95$) and coated ($\varepsilon = 0.9$) fibers as a function of fiber diameter before coating (Langmuir relation used, approach velocity = 5 cm/s).

*Effect of Coating on Adsorption*

The previously implemented adsorption model (the homogenous solid diffusion model) was exercised to determine the effect of fiber diameter and approach velocity on adsorption performance of the coated fibers. The analyses assumed an equal volume of fiberglass and adsorbent. That is, the overall porosity of the adsorbing medium was 90% with 5% of the volume occupied by the original fiberglass medium and 5% of the volume occupied by the adsorbent coating. Since the effective diffusion coefficient of the adsorbate and adsorbent are unknown we attempted to capture a worst case situation by assigning a relatively low diffusion coefficient of 5e-13 $m^2/s$. Higher effective diffusion should only improve the adsorption efficiency of the adsorbent.

Results are shown in Figures 10-12 below. In Figure 10 the normalized adsorbate mass fraction exiting the bed is shown for a range of (uncoated) fiber diameters ranging from 2 to 20 microns and an approach velocity of 1.6 cm/s. We can see a significant difference in the performance of fibers of varying diameter. This is displayed a little more clearly in Figure 11 where the time to reach a breakthrough concentration of 1% of the incoming concentration is plotted against the original fiber diameter. We see a continuous decrease in breakthrough time as fiber diameter is increased from 2 to 20 μm but the drop-off from 2 μm to 10 μm is less than 10% (a reduction in breakthrough time from 48.5 s to 44 s).

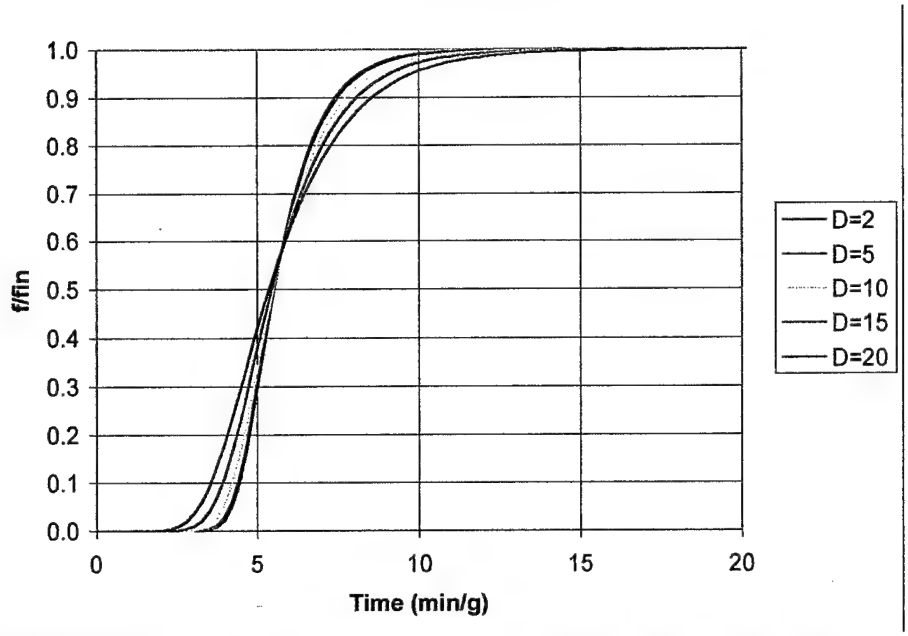


Figure 10. Breakthrough curves for coated fibers of varying sizes (size shown is diameter, in microns, of the glass fiber before coating).

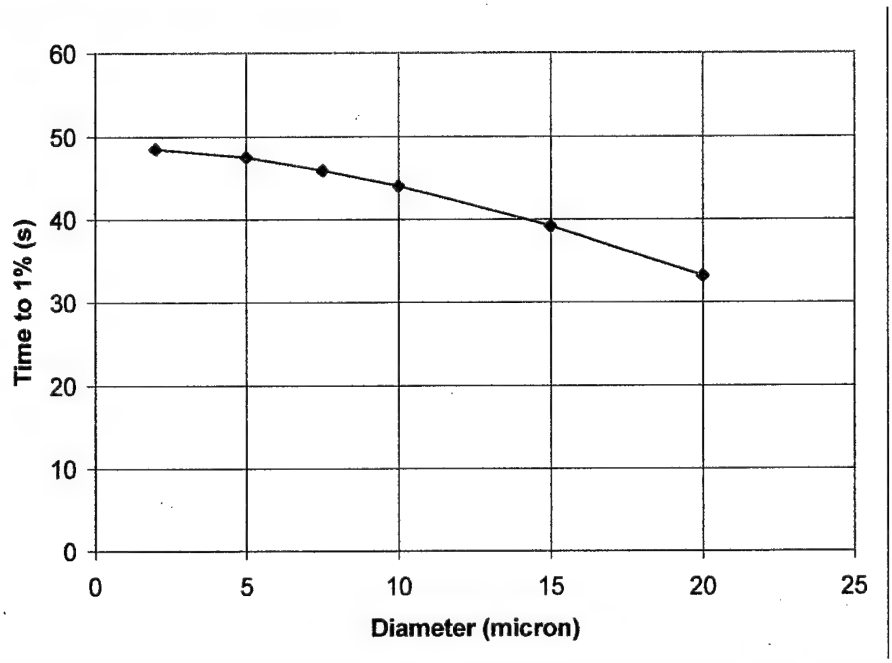


Figure 11. Variation of initial breakthrough time with original (uncoated) fiber diameter

The previous analyses were repeated at a higher approach velocity of 4.8 cm/s. This upper bound was chosen, as it is a typical maximum for HEPA filter media. The previously predicted pattern of degradation of adsorption performance with increasing fiber diameter was seen to continue. The higher the approach velocity the poorer is the adsorption performance of the fibers of larger diameter. Results are shown in Figure 12 where the normalized time to reach an adsorbate exit concentration of 1% of the influent concentration is plotted as a function of (uncoated) fiber diameter. Curves are shown for approach velocities of 1.6 cm/s and 4.8 cm/s. We see a

continuous decrease in breakthrough time as fiber diameter is increased from 2 to 20 μm and we see a larger rate of decline as the approach velocity increases. However, up to a fiber size of 5 μm the adsorption behavior is virtually the same for the two velocities. Therefore, from the standpoint of adsorption efficiency the performance of the 5 μm fibers is almost as good as that of the 2 μm fibers. At a fiber size of 10 μm and an approach velocity of 5 cm/s the breakthrough time is less than 80% of the breakthrough time for 2 μm fibers.

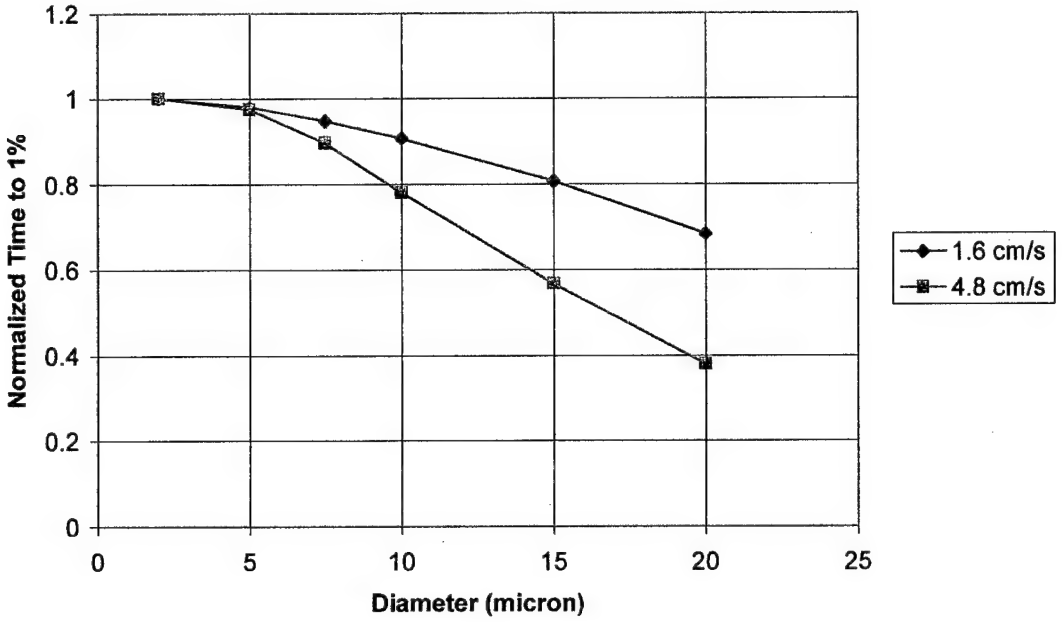


Figure 12. Variation of initial breakthrough time (normalized) with original (uncoated) fiber diameter and approach velocity.

While the adsorption behavior of 2 and 5 μm fibers is nearly the same there is a significant difference in the pressure drop between the two fiber sizes. This is shown in Figure 9 where the pressure drop through a fibrous mat of 0.8 mm thickness with an approach velocity of 5 cm/s is shown. For the 2 μm fibers the pressure drop will be about 14 mm $H_2O$ while for the 5 μm fibers it will be about 2.5 mm $H_2O$, a factor of nearly 6.

## Summary

The adsorption model and the bed resistance model were incorporated into CFD-ACE and tested and demonstrated. The pressure drop and adsorption models were then exercised to simulate behavior of coated fibers under conditions that might be typical of gas mask conditions. These analyses indicate that there is a reduction in adsorption performance as fiber diameter increases. At a diameter (before coating) of 5 μm adsorption performance is almost as good as that of 2 μm fibers. Beyond 5 μm the adsorption performance starts to fall off rapidly. Since the 5 μm diameter fiber will result in less pressure drop than the 2 μm fiber diameter, the larger size is recommended. If better air filtration performance is desired the base fiber size could be decreased with a corresponding increase in pressure drop.

## References


1. Marsh, H. and Rand, B., "The Characterization of Microporous Carbons by Means of the Dubinin-Radushkevich Equation," Journal of Colloid and Interface Science, Vol 33, No. 1, 1970.

2. Mangun, C. L., Braatz, R. D., Economy, J. and Hall, A. J., "Fixed Bed Adsorption of Acetone and Ammonia onto Oxidized Activated Carbon Fibers."

3. Johnson, Richard W., The Handbook of Fluid Dynamics, 1998

4. Dullien, F. A. L., **Porous Media, Fluid Transport and Pore Structure**, 2nd Edition, Academic Press, 1992.

5. Kyan, C. P., Wasan, D. T. and Kintner, R. C., "Flow of Single-Phase Fluids through Fibrous Beds, Ind. Eng. Chem. Fundam., Vol. 9, No. 4, 1970.

6. Chen, C. Y., "Filtration of Aerosols by Fibrous Media," Chem. Review, 55, 595, 1955.


## EKOS Materials Corp.

Due to the stringent requirements of the gas mask, EKOS worked on the development of several novel ACF materials to improve the adsorption capacity and find ways to reduce size and pressure drop. The most promising concept explored was coating HEPA microfiber glass mats with an appropriate resin followed by activation. The current gas mask canister is composed of two parts, a HEPA filter and a bed of ASZM-TEDA granular activated carbon, which contribute roughly the same amount to the pressure drop. Thus it was anticipated that by utilizing a carbon coated HEPA, we could achieve filtration and adsorption in a single stage with reduced pressure drop. However, to maximize our chance of success, several paths were explored.

*Chemical Activation*

The most promising avenue has been the development of a new low temperature route (350°C) to activate the samples using zinc chloride as a strong dehydration catalyst. The advantages of this method are a wide range of surface areas can be made, the glass mats are much more resilient, and we believe the zinc chloride reduces to zinc oxide after activation which is useful as an acidic gas scavenger. Samples produced in this manner have the structural integrity for testing but lack the basic functional groups to adsorb the acidic molecules (ASZM carbons tested without TEDA present showed very poor breakthrough against CK). We have tried a variety of methods to react the phenolic coating with ammonia but it appears that 350°C is just too low of temperature. Thus, for one set of experiments, we have switched to using PAN as the precursor and shown that we can produce high surface areas while leaving the majority of the basic nitrile groups intact. As an interesting side note, we believe that this new activation method could be utilized to coat polymeric fibers with activated carbon to produce an extremely flexible material

that could be used in such applications as protective clothing. From this research, a patent has been applied for and granted in the U.S.

Sample Preparation and Testing

*E-glass mats with metal impregnants*

E1 was prepared using phenolic resin with addition of zinc and copper oxide followed by activation in ammonia at 600C to impart basic functional groups (50wt% carbon with SA~100 $m^2/g$ due to high loading). E2 was prepared in the same way but using a lower amount of metal impregnants (50wt% carbon and SA of 530 $m^2/g$). The addition of ACF layers at the end of a bed of ASZM leads to increased breakthrough as shown in the following graph. If we examine the time to breakthrough at a CK concentration of 8 $mg/m^3$ (which is considered the end point by the Army) and the bed thickness, we find that ASZM has a CK equivalent of 3.15 min/mm while E2 has 14.55 min/mm. This is a significantly better adsorption capacity per bed thickness even taking into account the typical deviation of ASZM breakthrough time (Dave Tevault reports it can vary by up to 20% for CK). Thus the results we are measuring appear to be outside the error bars and would account for a real increase in time to breakthrough.

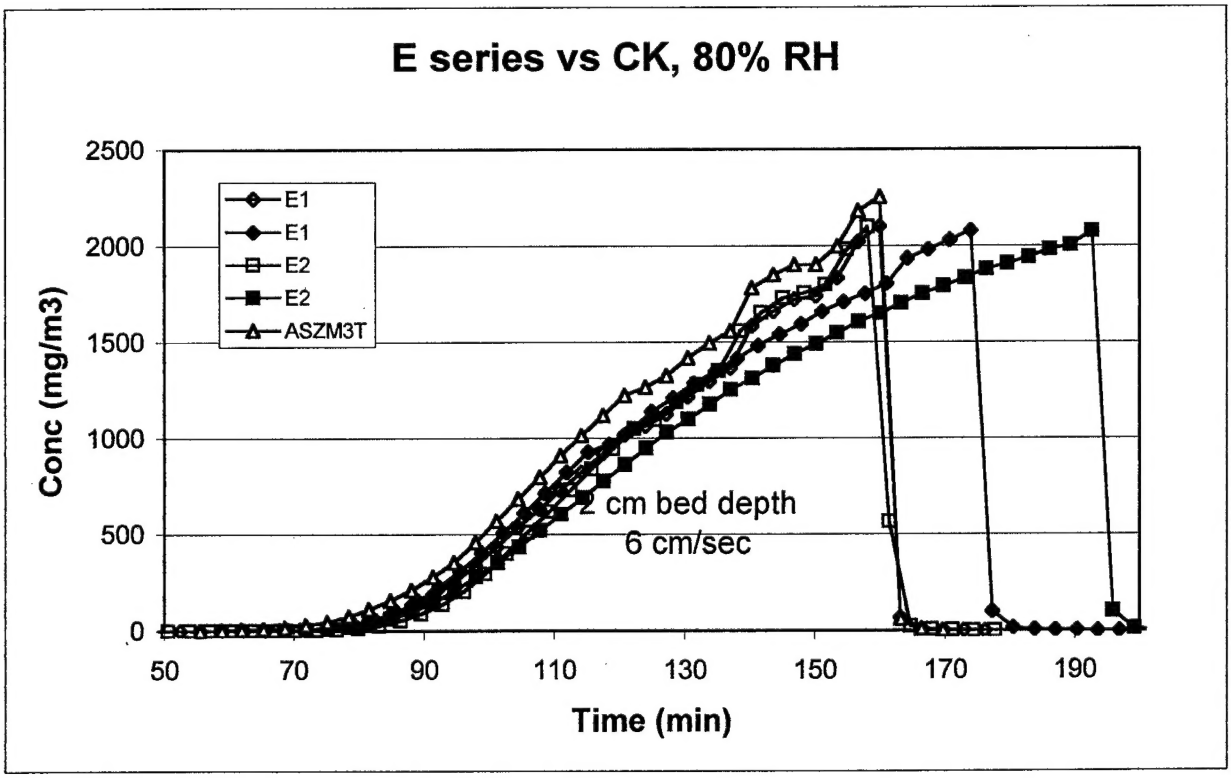


*HEPA glass mats*

H1 was prepared using phenolic resin with $ZnCl_2$ followed by activation at 350C in nitrogen (39wt% carbon with SA of 1280 $m^2/g$). E2 was prepared in a similar manner but with increased carbon content (54wt% carbon and SA of 845 $m^2/g$). Again we see an increase in time to

breakthrough but here the ASZM has an equivalent of 2.29 min/mm as compared to 18.8 min/mm for the H2. This type of difference does give confidence that we are outside the range of experimental error and have produced a much better adsorbent material. It is also obvious that the ZnO leftover from activation has a beneficial effect on breakthrough time.

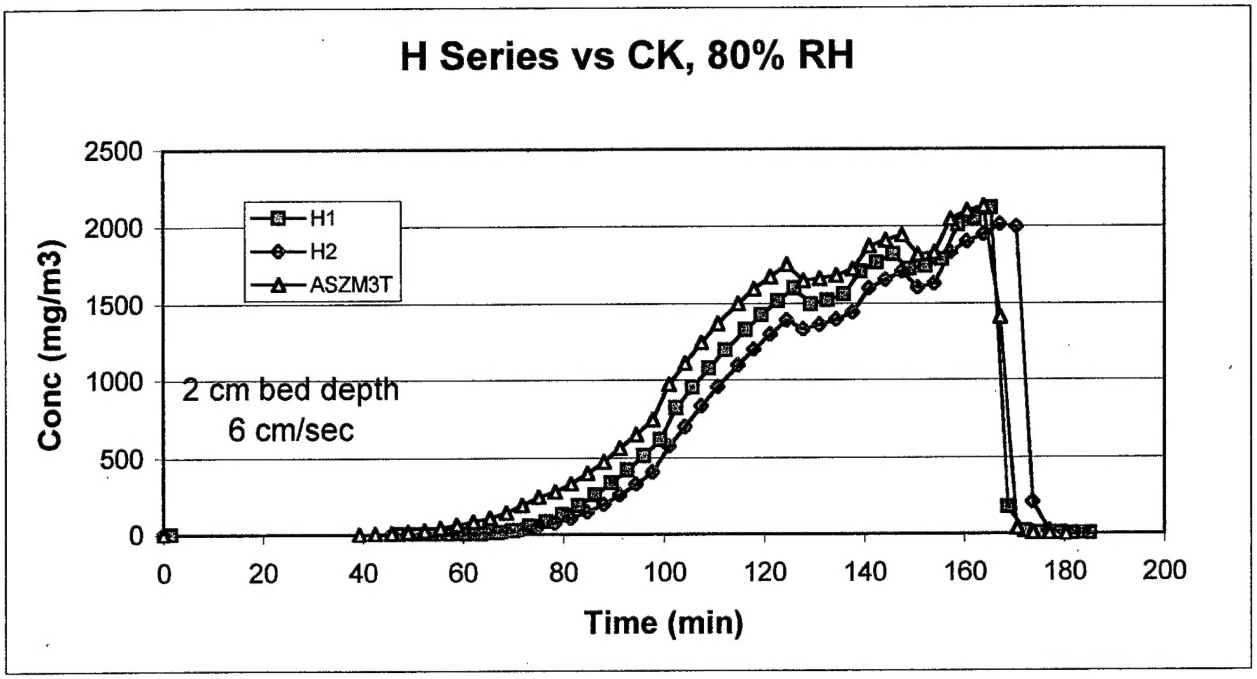


The next step was to test an entire bed of just ACF, H&V produced larger quantities of the thick HEPA materials that were then activated by EKOS and sent to Edgewood for testing. X3 has been coated with phenolic resin then activated in ammonia to achieve small basic pores for maximum adsorption of CK, impregnated with zinc/copper to achieve catalytic decomposition of CK (we expect the strong basic groups which are chemically bonded to the carbon edge sites to supplant the TEDA which is currently used). This was carried out by incorporating particulates of zinc and cupric oxide into the resin solution before coating; surface area measurements were completed which indicate minimal pore blockage by the metal particles. This is a greatly simplified process as compared to current GAC impregnation techniques. CK breakthrough testing on several layers is shown below. The curves are very unusual in that immediate breakthrough is seen with the 7 and 14 layers tests while the 23 layer bed has a breakthrough time comparative to the ASZM carbon. There must be severe short circuiting around the edges of the bed to display this type of behavior. Unfortunately, additional sets of ACF that were tested also displayed similar results (including the samples utilizing PAN with and without ZnO&CuO). It was thought that the high pressure drops of the samples led to such behavior, as the gas would be more apt to go ahead rather than through the sample.

To make the HEPA process viable, better processing would be required to keep the pressure drop low while still retaining good particulate removal. Potential methods to accomplish this goal such as vacuum impregnation to reduce webbing and pre-coating the fibers before incorporation into a nonwoven mat would require a large manufacturing partner.

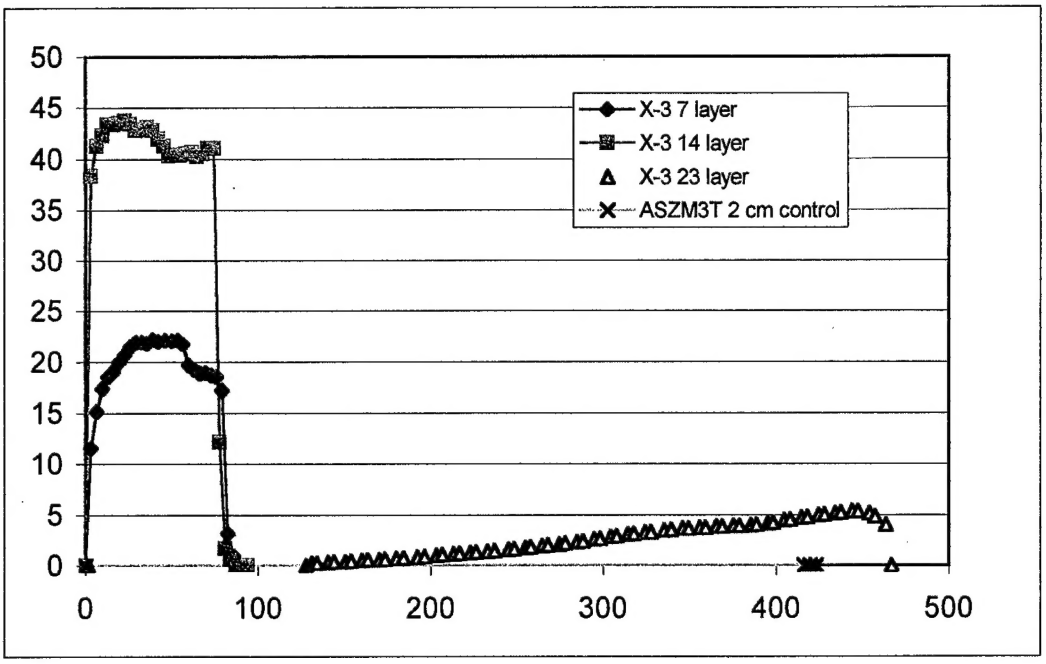


*Designed Microstructures*

CCI produced a series of ceramic-based designed structures using stereolithography. EKOS has successfully coated these discs (both octet truss and honeycomb) with phenolic resin containing either catalytic metals or ASZM PAC followed by activation in ammonia. Testing of 2cm bed depths for CK breakthrough showed poor results as either a sufficient mass transfer zone could not be established or contact efficiency was impeded due to lack of turbulence.

TOTAL PROJECT COST: $ 539,738

UNUSED FUNDS: $ 53,401

The Contractor, EKOS Materials Corp., hereby declares that, to the best of its knowledge and belief, the technical data delivered herewith under Contract No. DAAH01-99-C-R175 is complete, accurate, and complies with all requirements of the contract.

Date 3/21/03

Name and Title of Authorized Official Christian Mangun - President